

# Deep Learning for Nonlinear Diffractive Imaging

Yu Sun\*, Zhihao Xia\*, and Ulugbek S. Kamilov\*

July 16, 2022

## Abstract

Image reconstruction under multiple light scattering is crucial for a number of important applications in cell microscopy and tissue imaging. The reconstruction problem is often formulated as a nonconvex optimization, where a nonlinear measurement model is used to account for multiple scattering and a regularizer is used to enforce the prior on the object. In this letter, We propose a powerful alternative to this optimization-based view of image reconstruction by designing and training a deep convolutional neural network (CNN) for inverting multiple scattering. Simulations show that the proposed formulation is substantially faster and achieves higher imaging quality compared to the state-of-the-art methods based on optimization.

## 1 Introduction

The problem of reconstructing the spatial distribution of the dielectric permittivity of an unknown object from the measurements of the light it scatters is common in many applications such as tomographic microscopy [1] and digital holography [2]. The problem is often formulated as a linear inverse problem by adopting scattering models based on the first Born [3] or Rytov [4] approximations. However, these linear approximations are inaccurate when scattering is strong, which leads to reconstruction artifacts for objects that are large or have high permittivity contrasts [5]. For strongly scattering objects, it is preferably to use nonlinear measurement models that can account for multiple light scattering inside the object [6–9].

When adopting a nonlinear measurement model, it is common to formulate image reconstruction as an optimization problem. The objective function in the optimization typically includes two terms: a smooth data-fidelity term that ensures that the final image is consistent with measured data, and a regularizer that mitigates the ill-posedness of the problem by promoting solutions with desirable properties [10]. For example, one of the most widely adopted regularizers is total variation (TV), which preserves image edges while promoting smoothness [11]. TV is often interpreted as a sparsity-enforcing  $\ell_1$ -penalty on the image gradient and has proven to be successful in the context of imaging from scattered light measurements [12–15].

Despite the recent progress in regularized image reconstruction under multiple scattering, the corresponding optimization problem is difficult to solve. The challenging aspects are the nonconvex nature of the objective and the large amount of data that needs to be processed in typical imaging applications. In particular, when the scattering is strong, the problem becomes highly nonconvex, which negatively impacts both the speed of reconstruction and the quality of the final estimate [15].

In this letter, we consider a fundamentally different approach to the problem of image reconstruction under multiple scattering. Recently, several results have indicated that multiple light scattering can be interpreted as a forward-pass of a convolutional neural network (CNN) [16–18]. This view suggests that the

---

\*Y. Sun (email: sun.yu@wustl.edu) and Z. Xia (email: zhihao.xia@wustl.edu) are with the Department of Computer Science and Engineering (CSE), Washington University in St. Louis, St. Louis, MO 63130, USA. U. S. Kamilov (email: kamilov@wustl.edu) is with the Department of Computer Science and Engineering (CSE) and with the Department of Electrical and Systems Engineering (ESE), Washington University in St. Louis, St. Louis, MO 63130, USA.

scattered light measurements at the sensor locations can be interpreted as an encoding of the dielectric permittivity with a CNN governing the light propagation. Based on this observation, we propose to reconstruct the object by designing another CNN that is trained to invert the multiple scattering in a data-driven fashion. While our approach is consistent with the recent trend of using deep learning architectures for image reconstruction [19–26], it is fundamentally different in the sense that our measurement operator is both nonlinear and object dependent (and hence unknown). Our approach is also related to the recent work on reverse photon migration for diffuse optical tomography [27]. However, our focus is on diffractive imaging, where the light propagation is assumed to be deterministic, rather than stochastic as in [27]. Our simulations show that it is possible to invert multiple light scattering by training a CNN, even when imaging strongly scattering objects where optimization-based approaches fail. To the best of our knowledge, the results here are the first to show the potential of deep learning to reconstruct high-quality images from multiply scattered light measurements.

## 2 Nonlinear Diffractive Imaging

In this section, we describe the traditional optimization-based approach for nonlinear diffractive imaging. We first review the image reconstruction and then discuss the details of the physics of forward light scattering.

### 2.1 Nonlinear Inverse Problem

We consider an imaging inverse problem

$$\mathbf{y} = \mathbf{H}(\mathbf{x}) + \mathbf{e}, \quad (1)$$

where the goal is to recover the unknown image  $\mathbf{x} \in \mathbb{R}^N$  from the noisy measurements  $\mathbf{y} \in \mathbb{C}^M$ . The measurement operator  $\mathbf{H} : \mathbb{R}^N \rightarrow \mathbb{C}^M$  models the response of the imaging system and the vector  $\mathbf{e} \in \mathbb{C}^M$  represents the measurement noise, which is often assumed to be independent and identically distributed (i.i.d.) Gaussian. When the inverse problem is linear, the measurement operator is represented as a measurement matrix  $\mathbf{H} \in \mathbb{C}^{M \times N}$ .

In practice, problems such as (1) are often ill-posed; the standard approach for solving them is by formulating an optimization problem

$$\hat{\mathbf{x}} = \arg \min_{\mathbf{x} \in \mathbb{R}^N} \left\{ \frac{1}{2} \|\mathbf{y} - \mathbf{H}(\mathbf{x})\|_{\ell_2}^2 + \mathcal{R}(\mathbf{x}) \right\}, \quad (2)$$

where the data-fidelity term ensures that the final image is consistent with measured data and the regularizer  $\mathcal{R}$  promotes solutions with desirable properties. Two common regularizers for images include the spatial sparsity-promoting penalty  $\mathcal{R}(\mathbf{x}) \triangleq \tau \|\mathbf{x}\|_{\ell_1}$  and total variation (TV) penalty  $\mathcal{R}(\mathbf{x}) \triangleq \tau \|\mathbf{D}\mathbf{x}\|_{\ell_1}$ , where  $\mathbf{D}$  is the discrete gradient operator [11, 28, 29]. Two common methods for solving optimization problems of form (2) are FISTA [30] and ADMM [31], both of which were successfully applied to the problem of image reconstruction from scattered light data [15].

### 2.2 Forward Light Scattering

Consider the scattering problem illustrated in Fig. 1, where an object of the permittivity distribution  $\epsilon(\mathbf{r})$  in the bounded domain  $\Omega \subseteq \mathbb{R}^2$  is immersed into a background medium of permittivity  $\epsilon_b$  and illuminated with the incident electric field  $u_{\text{in}}(\mathbf{r})$ . We assume that the incident field is monochromatic and coherent, and it is known inside  $\Omega$  and at the locations of the sensors. The result of object-light interaction is measured at the location of the sensors as a scattered field  $u_{\text{sc}}(\mathbf{r})$ . The multiple scattering of light can be accurately described by the Lippmann-Schwinger equation [32] inside the image domain

$$u(\mathbf{r}) = u_{\text{in}}(\mathbf{r}) + \int_{\Omega} g(\mathbf{r} - \mathbf{r}') f(\mathbf{r}') u(\mathbf{r}') \, d\mathbf{r}', \quad (\mathbf{r} \in \Omega) \quad (3)$$

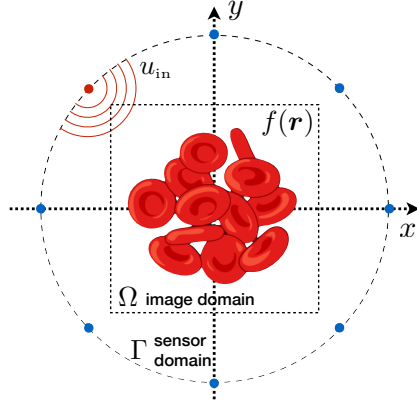


Figure 1: Schematic representation of scattering scenarios considered in this letter. An object of a scattering potential  $f(r)$  is illuminated with an input wave  $u_{\text{in}}$ , which interacts with the object and leads to the scattered field  $u_{\text{sc}}$  at the sensors.

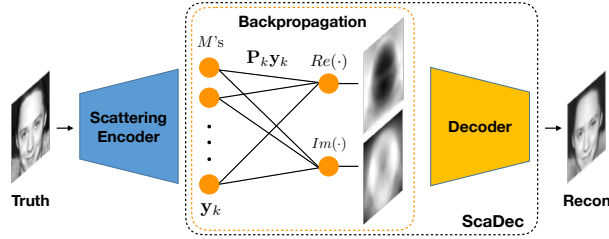


Figure 2: The overview of the proposed image reconstruction framework that first backpropagates the data into a complex valued image and transforms this image into the final image with a CNN.

where  $u(\mathbf{r}) = u_{\text{in}}(\mathbf{r}) + u_{\text{sc}}(\mathbf{r})$  is the total electric field,  $f(\mathbf{r}) \triangleq k^2(\epsilon(\mathbf{r}) - \epsilon_b)$  is the scattering potential, which is assumed to be real, and  $k = 2\pi/\lambda$  is the wavenumber in vacuum. The function  $g(\mathbf{r})$  is the Green's function, defined as

$$g(\mathbf{r}) \triangleq \frac{j}{4} H_0^{(1)}(k_b \|\mathbf{r}\|_{\ell_2}) \quad (4)$$

where  $k_b \triangleq k\sqrt{\epsilon_b}$  is the wavenumber of the background medium and  $H_0^{(1)}$  is the zero-order Hankel function of the first kind. Note that the knowledge of the total-field  $u$  inside the image domain  $\Omega$  enables the prediction of the scattered field at the sensor domain

$$u_{\text{sc}}(\mathbf{r}) = \int_{\Omega} g(\mathbf{r} - \mathbf{r}') f(\mathbf{r}') u(\mathbf{r}') d\mathbf{r}'. \quad (\mathbf{r} \in \Gamma) \quad (5)$$

The discretization and combination of (3) and (5) leads to the following matrix-vector description of the scattering problem

$$\mathbf{y} = \mathbf{S}(\mathbf{u} \cdot \mathbf{x}) + \mathbf{e} \quad (6a)$$

$$\mathbf{u} = \mathbf{u}_{\text{in}} + \mathbf{G}(\mathbf{u} \cdot \mathbf{x}), \quad (6b)$$

where  $\mathbf{x} \in \mathbb{R}^N$  is the discretized scattering potential  $f$ ,  $\mathbf{y} \in \mathbb{C}^M$  is the measured scattered field  $u_{\text{sc}}$  at  $\Gamma$ ,  $\mathbf{u}_{\text{in}} \in \mathbb{C}^N$  is the input field  $u_{\text{in}}$  inside  $\Omega$ ,  $\mathbf{S} \in \mathbb{C}^{M \times N}$  is the discretization of the Green's function at  $\Gamma$ ,  $\mathbf{G} \in \mathbb{C}^{N \times N}$  is the discretization of the Green's function inside  $\Omega$ ,  $\cdot$  denotes a component-wise multiplication

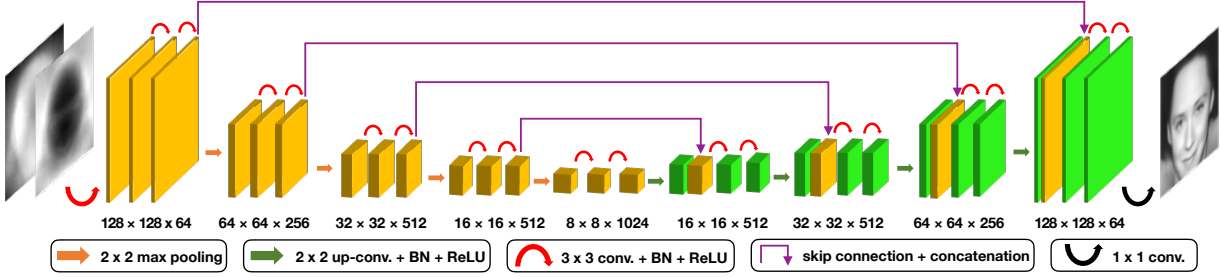


Figure 3: Visual illustration of the proposed learning architecture based on U-Net. The input consists of two channels that correspond to the real and imaginary parts of the backpropagated vector  $\mathbf{w} \in \mathbb{C}^N$ . The output is a single image of the scattering potential  $\mathbf{x} \in \mathbb{R}^N$ .

between two vectors, and  $\mathbf{e} \in \mathbb{C}^M$  models the additive noise at the measurements. Using the shorthand notation  $\mathbf{A} \triangleq \mathbf{I} - \text{Gdiag}(\mathbf{x})$ , where  $\mathbf{I} \in \mathbb{R}^{N \times N}$  is the identity matrix and  $\text{diag}(\cdot)$  is an operator that forms a diagonal matrix from its argument, we can formally specify the nonlinear forward model as follows

$$\mathbf{H}(\mathbf{x}) \triangleq \mathbf{S}(\mathbf{u}(\mathbf{x}) \cdot \mathbf{x}) \quad (7a)$$

where

$$\mathbf{u}(\mathbf{x}) \triangleq \arg \min_{\mathbf{u} \in \mathbb{C}^N} \left\{ \frac{1}{2} \|\mathbf{A}\mathbf{u} - \mathbf{u}_{\text{in}}\|_{\ell_2}^2 \right\} \quad (7b)$$

The recent work has shown that the computation of the operator  $\mathbf{H}$  can be interpreted as a CNN and that the gradient of the corresponding data-fidelity term can be efficiently evaluated, which enables efficient optimization [15–18].

### 3 Scattering Decoder

We next describe the proposed alternative based on deep learning. We refer to our reconstruction approach as the *Scattering Decoder (ScaDec)*.

#### 3.1 Backpropagation to the image domain

The general framework of our approach is visually illustrated in Figure 2. The first-step in the method is backpropagation, which simply transforms the collected measurements from the measurement domain to the image domain. We define the backpropagation of the measurements generated by one transmitter as

$$\mathbf{z} = \mathbf{P}\mathbf{y} \quad \text{with} \quad \mathbf{P} \triangleq \text{diag}(\mathbf{u}_{\text{in}}^*)\mathbf{S}^H, \quad (8)$$

where  $\mathbf{y} \in \mathbb{C}^M$  are the measurements generated by one transmitter and collected by  $M$  receivers, and  $\mathbf{P} \in \mathbb{C}^{N \times M}$  are the backpropagation operator. The matrix  $\mathbf{S}^H \in \mathbb{C}^{N \times M}$  is the Hermitian transpose of the discretized Green's function  $\mathbf{S}$  evaluated at  $\Gamma$ , and  $\mathbf{u}_{\text{in}}^*$  is the element-wise conjugate of the  $\mathbf{u}_{\text{in}}$ . The output  $\mathbf{z} \in \mathbb{C}^N$  is a complex vector with  $N$  elements corresponding to the number of pixels in the original image. When the data was collected with multiple transmissions, we define the backpropagation of multiple transmitters as

$$\mathbf{w} = \sum_{k=1}^K \mathbf{z}_k = \sum_{k=1}^K \mathbf{P}_k \mathbf{y}_k, \quad (9)$$

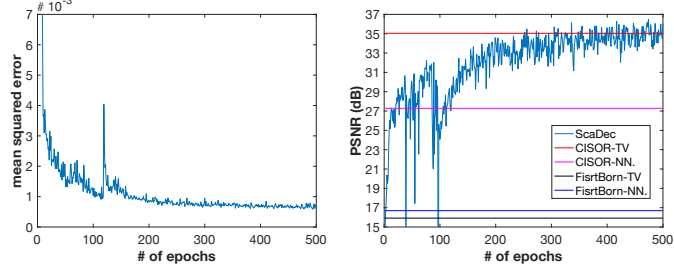


Figure 4: Illustration of the convergence of the training process on the dataset of piece-wise smooth objects. The left figure shows the training loss. The right figure shows the PSNR of the validation set during training. Horizontal lines show the performance of various other algorithms on the same data.

Table 1: PSNR (dB) comparison of five methods on two datasets

Piece-wise Smooth Objects					
	FB-NN	CISOR-NN	FB-TV	CISOR-TV	ScaDec
Scenario 1	27.32	27.32	34.97	34.97	<b>36.38</b>
Scenario 2	16.69	27.28	15.92	35.04	<b>36.38</b>
Celebrity Faces					
	FB-NN.	CISOR-NN.	FB-TV	CISOR-TV	ScaDec
Scenario 3	11.16	11.16	23.02	23.02	<b>23.36</b>

where  $\mathbf{w} \in \mathbb{C}^N$  is the linear combination of  $\mathbf{z}_k$  and  $K$  denotes the number of transmitters. The  $\mathbf{P}_k$  and the  $\mathbf{y}_k$  correspond to the backpropagation of the  $k$ th transmitter. Note that backpropagation (9) does not rely on the actual forward model  $\mathbf{H}(\cdot)$  in (7a) which is nonlinear. Remarkable, as we shall see, our simple backpropagation followed by a specific CNN architecture will be sufficient to recover a high-quality image given multiply scattered measurements.

Note that since  $\mathbf{w}$  is complex vector, we treat its real and complex parts as two distinct image channels of the desired size and stack them as two feature maps. Thus, the backpropagation can be viewed as a fixed layer to the CNN with  $M$  inputs and two outputs before the CNN decoder (see Fig. 2). The weights of this fixed layer are characterized by  $\mathbf{P}_k$ 's, and the activation functions for the output nodes are  $\text{Re}(\cdot)$  and the  $\text{Im}(\cdot)$ , respectively.

### 3.2 U-Net Decoder

We design the ScaDec model based on the U-Net architecture [34], which was recently applied to various image reconstruction tasks including X-ray CT [24, 35]. Fig. 2.2 shows a detailed diagram of the proposed CNN architecture. The key property of the architecture is the fact that the decoder employs a contraction-expansion structure based on the max pooling and the up-convolution. This means that given a fixed size kernel ( $3 \times 3$  in our case), the effective receptive field increases as the input goes deeper into the network. We shall see in the next section the backpropagation and the CNN decoder can jointly invert the non-linear operator  $\mathbf{H}$ .

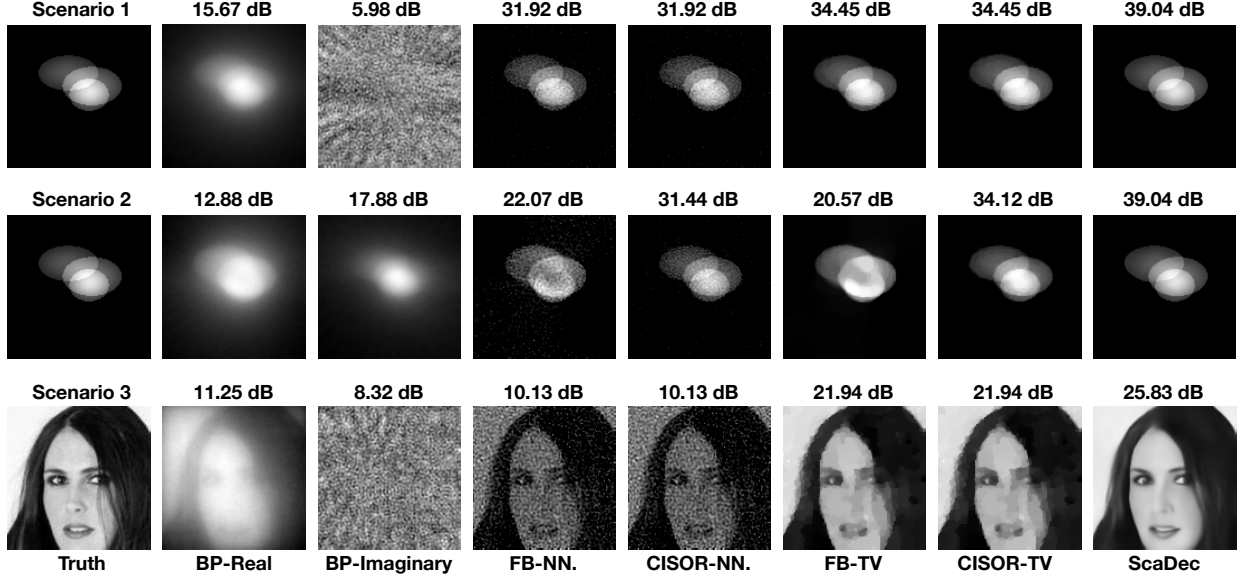


Figure 5: Visual comparison of the reconstructed images using the backpropagation (BP, columns 2-3), the linear model with first Born approximation regularized by imposing non-negativity [33] (FB-NN, column 4) and the total variation [12] (FB-TV, column 6), the non-linear CISOR method from [15] regularized by the non-negativity (CISOR-NN, column 5) and the total variation (CISOR-TV, column 7). The values above images show the PSNR (dB) of the reconstruction.

## 4 Experimental Validation

We now present the results of validating our method on two distinct sets of scattering data. Both datasets were obtained by using a high-fidelity simulation of the forward scattering problem with the conjugate-gradient solver. We validate the data-adaptive recovery capability of ScaDec by selecting datasets that consist of images with nontrivial features that are not well captured by fixed regularizers such as TV. In particular, the first dataset consists of synthetically generated piecewise-smooth images with sharp edges and smooth Gaussian regions. The second dataset [36] consists of human face images. Each of the datasets contains 1548 images, separated into 1500 images for training, 24 images for validation, and 24 images for testing. The physical size of images was set to  $18 \text{ cm} \times 18 \text{ cm}$ , discretized to a  $128 \times 128$  grid. The background medium is assumed to be air with  $\epsilon_b = 1$  and the wavelength of the illumination is set to  $\lambda = 0.84 \text{ cm}$ . The measurements are collected over 40 transmissions uniformly distributed along a circle of radius 1.6 m and, for each transmission, 360 measurements around the object are recorded. The simulated scattered data was additionally corrupted by an additive white Gaussian noise corresponding to 20 dB of input signal-to-noise ratio (SNR).

We considered two distinct scenarios corresponding to weak and strong scattering. In particular, we defined the permittivity contrast as  $f_{\max} \triangleq (\epsilon_{\max} - \epsilon_b)/\epsilon_b$ , where  $\epsilon_{\max} \triangleq \max_{\mathbf{r} \in \Omega} \{\epsilon(\mathbf{r})\}$ . The permittivity contrast quantifies the degree of nonlinearity in the inverse problem, with higher  $f_{\max}$  indicating stronger levels of multiple scattering. Scenario 1 corresponds to a weakly scattering regime with  $f_{\max} = 10^{-6}$ , while Scenario 2 considers strongly scattering regime with  $f_{\max} = 10^{-1}$ . For each scenario, we trained a separate ScaDec architecture using the corresponding training dataset with the loss function corresponding to the reconstruction mean squared error (MSE). This makes the proposed method favor solutions with higher peak signal-to-noise ratio (PSNR), which is widely used as a quality metric for images. As illustrated in Fig. 4, we observe no issues with the convergence of the training process. Note that all the PSNR and visual results were obtained on a distinct testing dataset.

Table 1 summarizes the results of comparing ScaDec against the baseline optimization-based methods corresponding to two distinct priors: nonnegativity constraints on the image and TV. For each prior, we consider the effects of the linearity versus nonlinearity of the forward model. The linear measurement model is obtained by using the first Born-approximation, while the nonlinear model takes into account multiple scattering by using the CISOR method [15]. Fig. 5 additionally shows some visual examples of the reconstructed images for each scenario under consideration. Note that the regularization parameters for TV were optimized for the best SNR performance for all the experiments.

The results confirm that as the level of scattering increases, the performance under the linear inverse problem formulation based on the first Born approximation degenerates with or without regularization. On the other hand, while TV regularization substantially improves the PSNR, it also leads to visible blocky artifacts in Fig. 5. On the other hand, the output of ScaDec substantially outperforms the baseline methods and leads to higher PSNR values and to more natural looking images free of blocky artifacts. ScaDec also enjoys remarkable stability in terms of performance, where the reconstruction PSNR is the same in weakly and strongly scattering regimes. Finally, the computational cost of ScaDec is extremely low during the testing stage, where each reconstruction corresponds to a simple forward pass through the CNN. These features make ScaDec a promising alternative to optimization based methods for reconstructing images from multiply scattered measurements.

## References

- [1] W. Choi, C. Fang-Yen, K. Badizadegan, S. Oh, N. Lue, R. R. Dasari, and M. S. Feld, “Tomographic phase microscopy,” *Nat. Methods*, vol. 4, no. 9, pp. 717–719, September 2007.
- [2] D. J. Brady, K. Choi, D. L. Marks, R. Horisaki, and S. Lim, “Compressive holography,” *Opt. Express*, vol. 17, no. 15, pp. 13 040–13 049, 2009.
- [3] E. Wolf, “Three-dimensional structure determination of semi-transparent objects from holographic data,” *Opt. Commun.*, vol. 1, no. 4, pp. 153–156, September/October 1969.
- [4] A. J. Devaney, “Inverse-scattering theory within the Rytov approximation,” *Opt. Lett.*, vol. 6, no. 8, pp. 374–376, August 1981.
- [5] B. Chen and J. J. Stamnes, “Validity of diffraction tomography based on the first born and the first rytov approximations,” *Appl. Opt.*, vol. 37, no. 14, pp. 2996–3006, May 1998.
- [6] K. Belkebir and A. Sentenac, “High-resolution optical diffraction microscopy,” *J. Opt. Soc. Am. A*, vol. 20, no. 7, pp. 1223–1229, July 2003.
- [7] K. Belkebir, P. C. Chaumet, and A. Sentenac, “Superresolution in total internal reflection tomography,” *J. Opt. Soc. Am. A*, vol. 22, no. 9, pp. 1889–1897, September 2005.
- [8] E. Mudry, P. C. Chaumet, K. Belkebir, and A. Sentenac, “Electromagnetic wave imaging of three-dimensional targets using a hybrid iterative inversion method,” *Inv. Probl.*, vol. 28, no. 6, p. 065007, April 2012.
- [9] T. Zhang, C. Godavarthi, P. C. Chaumet, G. Maire, H. Giovannini, A. Talneau, M. Allain, K. Belkebir, and A. Sentenac, “Far-field diffraction microscopy at  $\lambda/10$  resolution,” *Optica*, vol. 3, no. 6, pp. 609–612, June 2016.
- [10] A. Ribés and F. Schmitt, “Linear inverse problems in imaging,” *IEEE Signal Process. Mag.*, vol. 25, no. 4, pp. 84–99, July 2008.
- [11] L. I. Rudin, S. Osher, and E. Fatemi, “Nonlinear total variation based noise removal algorithms,” *Physica D*, vol. 60, no. 1–4, pp. 259–268, November 1992.

- [12] Y. Sung and R. R. Dasari, "Deterministic regularization of three-dimensional optical diffraction tomography," *J. Opt. Soc. Am. A*, vol. 28, no. 8, pp. 1554–1561, August 2011.
- [13] J. W. Lim, K. R. Lee, K. H. Jin, S. Shin, S. E. Lee, Y. K. Park, and J. C. Ye, "Comparative study of iterative reconstruction algorithms for missing cone problems in optical diffraction tomography," *Opt. Express*, vol. 23, no. 13, pp. 16 933–16 948, June 2015.
- [14] U. S. Kamilov, I. N. Papadopoulos, M. H. Shoreh, A. Goy, C. Vonesch, M. Unser, and D. Psaltis, "Optical tomographic image reconstruction based on beam propagation and sparse regularization," *IEEE Trans. Comp. Imag.*, vol. 2, no. 1, pp. 59–70, March 2016.
- [15] Y. Ma, H. Mansour, D. Liu, P. T. Boufounos, and U. S. Kamilov, "Accelerated image reconstruction for nonlinear diffractive imaging," in *Proc. IEEE Int. Conf. Acoustics, Speech and Signal Process. (ICASSP 2018)*, Calgary, Canada, April 15-20, 2018, arXiv:1708.01663 [cs.CV].
- [16] U. S. Kamilov, I. N. Papadopoulos, M. H. Shoreh, A. Goy, C. Vonesch, M. Unser, and D. Psaltis, "Learning approach to optical tomography," *Optica*, vol. 2, no. 6, pp. 517–522, June 2015.
- [17] U. S. Kamilov, D. Liu, H. Mansour, and P. T. Boufounos, "A recursive Born approach to nonlinear inverse scattering," *IEEE Signal Process. Lett.*, vol. 23, no. 8, pp. 1052–1056, August 2016.
- [18] H.-Y. Liu, D. Liu, H. Mansour, P. T. Boufounos, L. Waller, and U. S. Kamilov, "SEAGLE: Sparsity-driven image reconstruction under multiple scattering," *IEEE Trans. Comput. Imaging*, vol. 4, no. 1, pp. 73–86, March 2018.
- [19] C. Dong, C. C. Loy, K. He, and X. Tang, "Learning a deep convolutional network for image super-resolution," in *Proc. ECCV*, Zurich, Switzerland, September 6-12, 2014, pp. 184–199.
- [20] U. Schmidt and S. Roth, "Shrinkage fields for effective image restoration," in *Proc. IEEE Conf. Computer Vision and Pattern Recognition (CVPR)*, Columbus, OH, USA, June 23-28, 2014, pp. 2774–2781.
- [21] A. Mousavi, A. B. Patel, and R. G. Baraniuk, "A deep learning approach to structured signal recovery," in *Proc. Allerton Conf. Communication, Control, and Computing*, Allerton Park, IL, USA, September 30-October 2, 2015, pp. 1336–1343.
- [22] Y. Chen, W. Yu, and T. Pock, "On learning optimized reaction diffraction processes for effective image restoration," in *Proc. IEEE Conf. Computer Vision and Pattern Recognition (CVPR)*, Boston, MA, USA, June 8-10, 2015, pp. 5261–5269.
- [23] U. S. Kamilov and H. Mansour, "Learning optimal nonlinearities for iterative thresholding algorithms," *IEEE Signal Process. Lett.*, vol. 23, no. 5, pp. 747–751, May 2016.
- [24] K. H. Jin, M. T. McCann, E. Froustey, and M. Unser, "Deep convolutional neural network for inverse problems in imaging," 2016, arXiv:1611.03679 [cs.CV].
- [25] M. Borgerding and P. Schniter, "Onsanger-corrected deep networks for sparse linear inverse problems," 2016, arXiv:1612.01183 [cs.IT].
- [26] Y. S. Han, J. Yoo, and J. C. Ye, "Deep residual learning for compressed sensing CT reconstruction via persistent homology analysis," 2016, arXiv:1611.06391 [cs.CV].
- [27] J. Yoo, S. Sabir, D. Heo, K. H. Kim, A. Wahab, Y. Choi, S.-I. Lee, E. Y. Chae, H. H. Kim, Y. M. Bae, Y.-W. Choi, S. Cho, and J. C. Ye, "Deep learning can reverse photon migration for diffuse optical tomography," 2017, arXiv:1712.00912 [cs.CV].
- [28] E. J. Candès, J. Romberg, and T. Tao, "Robust uncertainty principles: Exact signal reconstruction from highly incomplete frequency information," *IEEE Trans. Inf. Theory*, vol. 52, no. 2, pp. 489–509, February 2006.

- [29] D. L. Donoho, “Compressed sensing,” *IEEE Trans. Inf. Theory*, vol. 52, no. 4, pp. 1289–1306, April 2006.
- [30] A. Beck and M. Teboulle, “Fast gradient-based algorithm for constrained total variation image denoising and deblurring problems,” *IEEE Trans. Image Process.*, vol. 18, no. 11, pp. 2419–2434, November 2009.
- [31] M. V. Afonso, J. M. Bioucas-Dias, and M. A. T. Figueiredo, “Fast image recovery using variable splitting and constrained optimization,” *IEEE Trans. Image Process.*, vol. 19, no. 9, pp. 2345–2356, September 2010.
- [32] M. Born and E. Wolf, *Principles of Optics*, 7th ed. Cambridge Univ. Press, 2003, ch. Scattering from inhomogeneous media, pp. 695–734.
- [33] Y. Sung, W. Choi, C. Fang-Yen, K. Badizadegan, R. R. Dasari, and M. S. Feld, “Optical diffraction tomography for high resolution live cell imaging,” *Opt. Express*, vol. 17, no. 1, pp. 266–277, December 2009.
- [34] O. Ronneberger, P. Fischer, and T. Brox, “U-net: Convolutional networks for biomedical image segmentation,” in *Medical Image Computing and Computer-Assisted Intervention (MICCAI)*, ser. LNCS, vol. 9351. Springer, 2015, pp. 234–241, (available on arXiv:1505.04597 [cs.CV]). [Online]. Available: <http://lmb.informatik.uni-freiburg.de/Publications/2015/RFB15a>
- [35] J. C. Ye, Y. Han, and E. Cha, “Deep Convolutional Framelets: A General Deep Learning Framework for Inverse Problems,” *ArXiv e-prints*, Jul. 2017.
- [36] Z. Liu, P. Luo, X. Wang, and X. Tang, “Deep learning face attributes in the wild,” in *Proceedings of International Conference on Computer Vision (ICCV)*, 2015.